

Non-equilibrium dynamics of the Holstein polaron driven by external electric field

Lev Vidmar,¹ Janez Bonča,^{1,2} Marcin Mierzejewski,^{3,1} Peter Prelovšek,^{1,2} and Stuart A. Trugman⁴

¹*J. Stefan Institute, 1000 Ljubljana, Slovenia*

²*Faculty of Mathematics and Physics, University of Ljubljana, 1000 Ljubljana, Slovenia*

³*Institute of Physics, University of Silesia, 40-007 Katowice, Poland*

⁴*Theoretical Division, Los Alamos National Laboratory, Los Alamos, New Mexico 87545, USA*

(Dated: March 5, 2022)

This Letter represents a fundamental study of a Holstein polaron in one dimension driven away from the ground state by a constant electric field. Taking fully into account quantum effects we follow the time-evolution of the system from its ground state as the constant electric field is switched on at $t = 0$, until it reaches a steady state. At weak electron phonon coupling (EP) the system experiences damped Bloch oscillations (BO) characteristic for noninteracting electron band. An analytic expression of the steady state current is proposed in terms of weak EP coupling and electric field. In the strong coupling limit weakly damped BO, consistent with nearly adiabatic evolution within the polaron band, persist up to extremely large electric fields.

PACS numbers: 63.20.kd, 72.10.Di, 72.20.Ht

Research in the field of non-equilibrium dynamics of complex quantum systems constitutes a formidable theoretical challenge. Many advanced numerical techniques, ranging from exact-diagonalization [1], expansion using Chebyshev polynomials [2], time-dependent density matrix renormalization group [3], to non-equilibrium dynamical mean field techniques [4] have been developed to tackle this complex problem.

More than forty years ago using a path-integral approach Thornber and Feynman[5] discovered that an electron in a parabolic band, driven by the electric field, acquires a constant velocity due to emission of phonons. Later approaches to polaron motion in high electric field used predominantly Boltzman equations [6], the high-field drift velocity was estimated via phonon-assisted hopping between different rungs of Wannier-Stark states using rate equations [7, 8]. In ref. [9] one-dimensional Holstein polaron problem in strong electric field has been mapped on a nonstandard Bethe lattice. It has been realized that keeping full quantum coherence between many-body states is crucial to obtain finite drift velocity for dispersionless optical phonons. Extensive research of polaron dynamics within the Su-Shrieffer-Heeger model has been conducted within the adiabatic approximation to describe properties of conjugated polymers that may be used in a variety of applications like molecular electronics or light-emitting diodes [10–12].

By choosing the Holstein hamiltonian as one of the simplest model systems describing the interaction between a fermion and phonons, we found numerically accurate results of the model away from equilibrium while maintaining full quantum description of phonons. We analyze the one-dimensional Holstein model with a single electron, threaded by a time-dependent flux:

$$H = -t_0 \sum_l (e^{i\theta(t)} c_l^\dagger c_{l+1} + \text{H.c.}) + g \sum_i n_i (a_i^\dagger + a_i) + \omega_0 \sum_i a_i^\dagger a_i, \quad (1)$$

where c_i^\dagger and a_i^\dagger are electron and phonon creation operators at site i , respectively, and $n_i = c_i^\dagger c_i$ is electron density. ω_0 denotes a dispersionless optical phonon frequency and t_0 nearest-neighbor hopping amplitude. Dimensionless EP coupling strength is $\lambda = g^2/2t_0\omega_0$. The constant electric field F that is switched on at time $t = 0$ enters the Hamiltonian in Eq. 1 through the time-dependent phase $\theta(t) = -Ft$ for $t \geq 0$. We measure electric field F in units of $[t_0/e_0a]$ where e_0 is the unit charge and a is the lattice distance. We furthermore measure time in units of $[\hbar/t_0]$. From here on we set $a = e_0 = \hbar = t_0 = 1$.

To solve the time-dependent Hamiltonian for a single electron coupled to phonon degrees of freedom we use an improved numerical method, originally introduced in Ref. [13], that led to numerically exact solutions of the polaron ground and low-lying excited state properties. The method constructs the variational Hilbert space (VHS) starting from the single-electron Bloch state $c_{\mathbf{k}}^\dagger |\emptyset\rangle$ with no phonons on an infinite lattice. The VHS is then generated by applying the off-diagonal terms of Hamiltonian (1)

$$\left\{ |\phi_{\mathbf{k},l}^{(N_h, M)}\rangle \right\} = (H_{\text{kin}} + H_g^M)^{N_h} c_{\mathbf{k}}^\dagger |\emptyset\rangle, \quad (2)$$

where H_{kin} and H_g correspond to the first and the second term of the Hamiltonian in Eq. 1, respectively. Parameters N_h and M determine the size of the VHS. In addition, $N_h - 1$ represents the maximum distance between the electron and the phonon quanta and $N_h * M$ is the maximum number of phonon quanta contained in the Hilbert space. The parameter $M > 1$ (Ref. [14]) ensures good convergence in the strong EP coupling regime that contains multiple phonon excitations. To reach weak coupling regime, $\lambda \ll 1$, we have as well constructed VHS with large $N_h = 40$, however with a limited maximum number of phonon quanta $N_{\text{phmax}} = 6$.

We start the time propagation from the initial (zero temperature) polaron ground state at $F = 0$ using the time-dependent Lanczos technique [15]. Since we are dealing with a single particle in an infinite system, we compute time-dependent average of the current operator $j(t) = \langle \hat{I}(t) \rangle$, where $\hat{I}(t) =$

$i \sum_l e^{-iFt} c_l^\dagger c_{l+1} - \text{H.c.}$. In the case of a time-independent field F , the time-integral of the current is directly related to a change of the total energy $\int_0^t j(t') dt' = \Delta h(t)/F = x(t)$ where $\Delta h(t) = \langle H(t) \rangle - \langle H(t=0) \rangle$ and $x(t)$ represents the travelled distance [16].

We first present results obtained near the noninteracting limit, *i.e.* at $\lambda = 0.01$, where $j(t)$ displays damped Bloch oscillations (BO) around $j(t \rightarrow \infty) > 0$, see Fig. 1(a). The period and the initial amplitude of BO at small t are consistent with BO of a free electron, denoted with thin dashed line in Fig. 1(a). Damping is due to inelastic scattering on phonons that is in turn reflected in a monotonic increase of the average phonon number $\langle n_{ph} \rangle$ with time, as depicted in Fig. 1(c). Damping is, however, not the most important consequence of inelastic scattering. Notably, $j(t)$ approaches a positive steady state current \bar{j} for $t > t_s \sim 4t_B$ and $6t_B$ at $F = 1/5$ and $F = 1/2$ respectively, where t_B denotes the Bloch oscillation period $t_B = 2\pi/F$. Note that $\bar{j} \ll j_{0\text{max}} = 2$. The dependence of the steady state current \bar{j} on F will be discussed further in the text. The steady state current as well emerges as a linear dependence of the total energy on time: $\Delta h(t) = F\bar{j}t$, see results in Fig. 1(e), where with increasing t , $\Delta h(t)$ approaches a straight line.

On a more technical side we note that to reach a steady state, the Hilbert space used in our calculation must contain large enough set of excited states that in turn represent the reservoir for the absorption of energy. For this reason, different Hilbert spaces were used, depending on the strength of EP coupling and the size of F , see as well caption of Fig. 1.

At a larger value of EP coupling, $\lambda = 0.2$, a somewhat different physical picture emerges, see results in Figs. 1(b,d) and (f). The main differences can be summarized as: i) BO become overdamped, ii) $j(t)$ remains positive at all t , and iii) $j(t)$ reaches a steady state after a short time $t_s \lesssim t_B$. Characteristic for a steady state are linear t dependences of $\langle n_{ph} \rangle$ and $\Delta h(t)$ in Figs. 1(d) and (f), respectively. Common to all cases presented in Fig. 1, is the emergence of a constant, steady state current for $t > t_s$.

In figure Fig. 2(a) and (b) we present current vs. time in the strong coupling regime, *i.e.* at $\lambda = 2.0$. At $F = 1/10$ (Fig. 2(a)) we observe nearly undamped BO as the polaron adiabatically follows the polaron band. Regular oscillations in $\langle n_{ph} \rangle$ and $\Delta h(t)$ in Figs. 2(c) and (e) portray polaron averages nearly identical to their ground state values at corresponding wavevectors $k = Ft = 2\pi t/t_B$. The response of the system to external field is nearly elastic, since $\Delta h(t = l * t_B) \sim 0$ for any integer value of l . The average current remains indistinguishable from zero within the largest time interval tested with our calculation, *i.e.* $t < 20t_B$.

In order to illuminate this behavior we note that in the strong coupling limit a large gap Δ exists in the polaron excitation spectrum being of the order of ω_0 . The low-energy polaron excitation spectrum is presented for $\omega_0 = 1$ and $\lambda = 2$ in the inset of Fig. 2(a) where a gap $\Delta \sim 0.64$ separates the polaron band from the excited polaron band [13, 17], located just below the continuum denoted by the grey area. At small

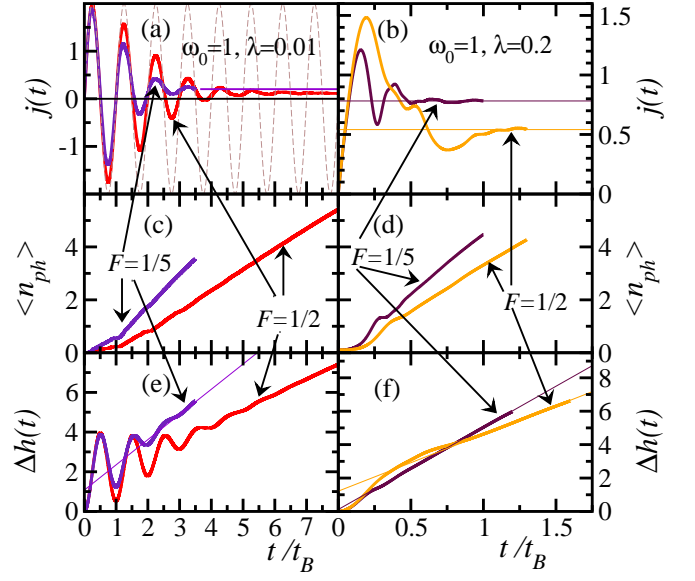


Figure 1: (Color online) $j(t)$ vs. t/t_B for two values of $F = 1/5$ and $1/2$ for $\omega_0 = 1$, and two distinct values of λ : a) $\lambda = 0.01$ and b) $\lambda = 0.2$. Thin dashed line in a) represents $j(t)$ for $\lambda = 0$, thin horizontal lines in a) and b) indicate steady-state values \bar{j} ; $\langle n_{ph} \rangle$ is shown in c) and d) for the same set of parameters as in a) and b), respectively; corresponding averages $\Delta h(t)$ are displayed in e) and f). The accuracy of time propagation was checked by comparison of the energy-gain sum rule $\Delta h(t) = F \int_0^t j(t') dt'$. Parameters, defining functional generator (Eq. 2) were $N_h = 40$, $M = 1$, and $N_{\text{phmax}} = 6$ for $F = 1/5$ and $N_h = 28$, $M = 1$ and $N_{\text{phmax}} = 8$ for $F = 1/2$. In this and all subsequent figures we used up to $N_{\text{st}} \sim 15 \times 10^6$ states in the Hilbert space and $N_{\text{step}} = 2000$ time steps within each t_B . Different sizes of VHS were used to check the convergence in the thermodynamic limit. Thin straight lines represent $t \rightarrow \infty$ extrapolations.

$F \ll \Delta$ there exist exponentially small probability for non-adiabatic transition from the polaron band to the excited polaron band or/and into the continuum.

For sufficiently large F ($F = 1/3$ and 1), see Figs. 2(b,d) and (f), BO in $j(t)$ lose periodicity even though remnants of BO remain clearly visible, and the time averaged current becomes finite (nonzero). Additional frequencies appear in $\langle n_{ph} \rangle$ that indicate multiple phonon excitations due to polaron transitions to excited polaron bands. Moreover, the average value of $\langle n_{ph} \rangle$ between successive t_B intervals increases. Total energy $\Delta h(t)$ as well increases in time. At large field, $F = 1$, $\Delta h(t)$ approaches a straight line signaling the onset of a steady state.

In Fig. 3 we follow the time evolution of the polaron at $F = 1/2$. We compute the average number of phonon quanta located at a given distance r from the electron $\gamma(r) = \langle \sum_i n_i a_{i+r}^\dagger a_{i+r} \rangle$, fulfilling the following sum-rule $\langle n_{ph} \rangle = \sum_r \gamma(r)$. At $t = 0$ $\gamma(r)$ displays a pronounced peak at the position of the electron, *i.e.* at $r = 0$, consistent with the shape of the polaron in its $k = 0$ ground state. After the electric field is switched on, $\gamma(r)$ experiences a compelling time evolution with three most outstanding characteristics: i) the over-

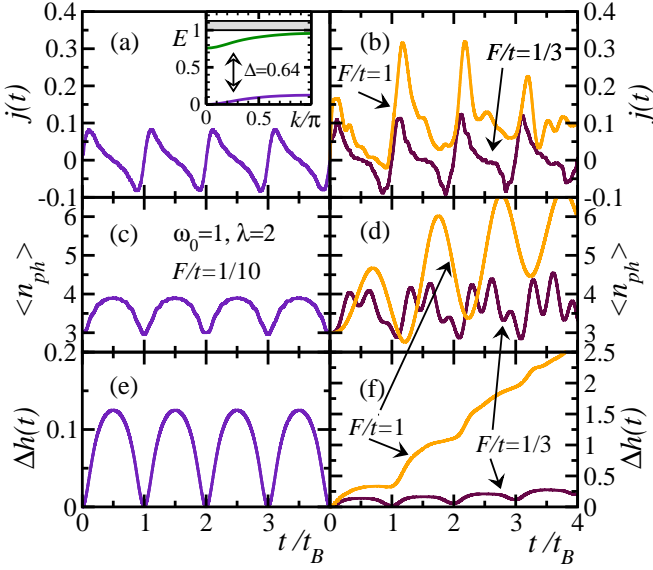


Figure 2: (Color online) $j(t)$ in a) and b), $\langle n_{ph} \rangle$ in c) and d), and $\Delta h(t)$ in e) and f) vs. t/t_B for $\omega_0 = 1$ and $\lambda = 2$ and three different values of F as indicated in figures. Insert in a) shows the polaron spectrum (ground state, first excited state energy and the continuum vs. the wavevector k) for $\omega_0 = 1$ and $\lambda = 2$. Note that there is a different vertical scale used in e) and f). We used $N_h = N_{phmax} = 20$ and $M = 1$ with $N_{st} = 3 \times 10^6$.

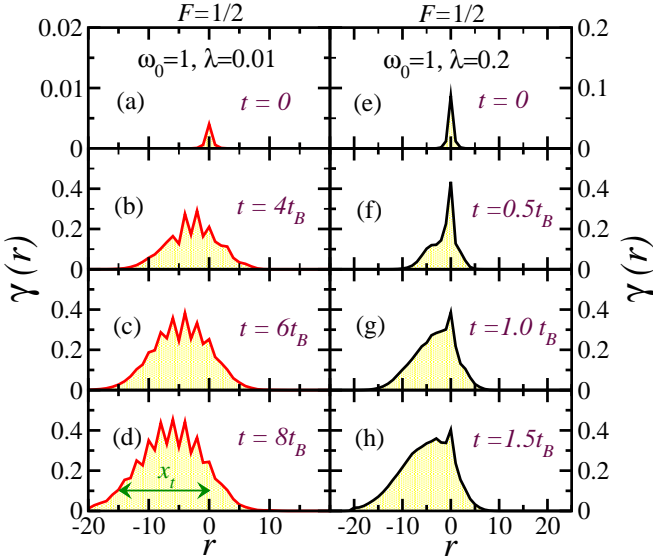


Figure 3: (Color online) $\gamma(r)$ for $\omega_0 = 1$, $\lambda = 0.01$ and $F = 1/2$ in a) through d) and $\lambda = 0.2$ in e) through h) computed at different times. The electric field is switched on at $t = 0$. Note a vertical scale change between a) and b) as well as between e) and f). x_t in (e) represents the travelled distance, see discussion in the text.

all increase of $\gamma(r)$ with time, ii) development of pronounced asymmetry of $\gamma(r)$ with respect to the electron position at $r = 0$, and iii) increased amount of polaron excitations in the forward direction. The overall increase of $\gamma(r)$ is consistent with the absorption of energy that is deposited in increasing

number of phonon excitations. The asymmetry is a result of a growing phonon tail, extending behind the moving polaron. Note that the polaron is moving from left towards right. In the long time limit, γ is expected to be approximately constant, independent of r and t , for r sufficiently negative. The average height of the polaron tail $\bar{\gamma}$ is due to energy conservation requirement independent of λ : $x(t)F \sim \langle n_{ph} \rangle \omega_0 \sim x(t) \bar{\gamma} \omega_0$, therefore $\bar{\gamma} \sim F/\omega_0$, compare Figs. 3(d) and (h). The length of the polaron tail is given by the expression for the travelled distance $x(t) = \Delta h(t)/F$. At $t = 8t_B$ and $\lambda = 0.01$ we obtain from Fig. 1(e) $x_t = x(8t_B) \sim 14.8$, that fits well with the length of the phonon tail in Fig. 3(d).

Rather unexpected is the pronounced increase of phonon excitations in the forward direction where $\gamma(r) \gtrsim 0$ up to $r \leq r_f \sim 5 - 7$ for all $t > 0$ presented in Fig. 3. Since time evolution starts from the ground state at zero temperature, there are no phonon excitations present far ahead from the moving electron. A substantial forward tail of phonon excitations is a consequence of damped BO. Indeed, r_f compares well with the Stark localization length, i.e. $r_f \sim L_S = 4/F = 8$. Yet another intriguing feature in $\gamma(r)$ emerges as regular oscillations in the polaron tail with a period $N_{hop} = \omega_0/F = 2$, clearly seen in the small $\lambda = 0.01$ limit, see Figs. 3(b) through (d). At larger $\lambda = 0.2$ these oscillations become overdamped.

The focal point of this Letter is calculation of the steady state current \bar{j} and analysis of its dependence on F and λ . In Fig. 4 we present \bar{j} vs. F for different values of λ . Note that the upper limit of \bar{j} is given by the current amplitude $j_{0max} = 2$ in the noninteracting system. We have limited our calculations to commensurate values of $F = \omega_0/N_{hop}$ with two exceptions: i) large $F > \omega_0$ where we have chosen $F = 2\omega_0, 3\omega_0, \dots$, and ii) results presented with disconnected triangles in Fig. 4(a), with details given in the figure caption. In the regime $\lambda \leq 0.1$, presented in Fig. 4(a), \bar{j} decreases with increasing F for $F \gtrsim 0.1$. Our method does not yield steady state results in the regime $F \lesssim 0.1$ due to large Stark localization length $L_S = 4/F$. Since $\bar{j} = 0$ for $F = 0$ as well as in the opposite limit, when $F \rightarrow \infty$, there must exist a global maximum value \bar{j}_{max} that depends on λ . For $\lambda = 0.1$, $\bar{j}_{max} \sim 0.82$, while for $\lambda < 0.1$, \bar{j}_{max} is reached somewhere in the interval $0 < F < 0.1$, not accessible by the present numerical method. Choosing rational or even irrational values of $1/F$ leads to a decrease of \bar{j} that nevertheless remains non-zero even in the latter case. A sweep over continuous values of F would lead to spikes in \bar{j} located at integer values of $1/F$, as consistent with observations in previous works [7–9].

To gain further insight into the decrease of \bar{j} with F , we plot in Fig. 4(b) $\bar{j}/\sqrt{\lambda}$ vs. $1/\sqrt{F}$ and realize that curves approximately collapse onto a straight line. The scaling can be qualitatively derived or argued in the following way: Let us consider only the commensurate case where $\omega_0/F = N_{hop} > 1$ is integer. If we use now the stationary representation of the problem, i.e. H where F enters the local potential energy as $H_F = -F \sum_i i n_i$, then the relevant eigenstates at $g = 0$ are Stark states which are localized within the typical length

$L_S = 4/F$. Applying Stark basis it becomes evident that $\bar{j} \rightarrow 0$ for $F \rightarrow \infty$ and arbitrary g . Considering only elastic processes conserving energy, $g \neq 0$ leads to hopping between different (orthogonal) Stark states being $N_{hop} < L_S$ sites apart and generating a phonon with $\omega_0 = FN_{hop}$. Effective matrix element for such process is $\tilde{t} \sim g/L_S$. Since a phonon can be generated anywhere within length L_S we are thus faced with a tight binding scheme with branching L_S at each step. Neglecting some possible differences in matrix elements the eigenvalues of such a problem are (coherently) propagating states $E_k \propto (g/\sqrt{L_S}) \cos(N_{hop}k)$ with the characteristic (maximum) velocity and current $\dot{j}_0 \propto v_{max} \propto gN_{hop}/\sqrt{L_S} \propto \sqrt{\frac{\lambda\omega_0^3}{F}}$. Even though the current amplitude \dot{j}_0 can not be directly compared to the average current \bar{j} , functional dependence of \bar{j} on λ and F is in good agreement with scaling in Fig. 4(b) that leads to $\bar{j} = \alpha \sqrt{\frac{\lambda\omega_0^3}{F}}$ with $\alpha \sim 0.89$ (fit is represented by a dashed line). Scaling breaks down when with decreasing F , \bar{j} approaches the maximum \bar{j}_{max} . In Fig. 4(c) we present results for larger $\lambda \in [0.2, 0.8]$. With increasing λ , the position of \bar{j}_{max} shifts towards larger values of F while it decreases in its magnitude.

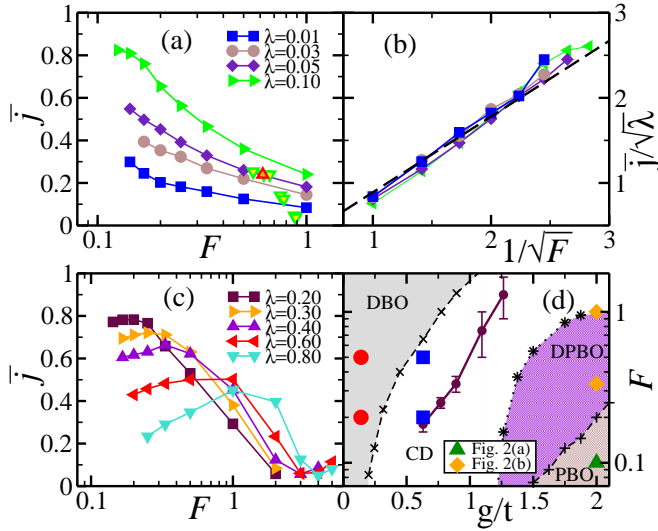


Figure 4: (Color online) Steady state current \bar{j} vs. F in the weak coupling limit in a) and in the weak to intermediate coupling regime in c), scaling $\bar{j}/\sqrt{\lambda}$ vs. $1/\sqrt{F}$ in the weak coupling limit in b), and diagram, presenting different regimes, as described in the text d). Also in d) circles with error bars indicate positions in the diagram where for a fixed g , a maximum value \bar{j}_{max} was reached; isolated circles, squares and diamonds indicate values used for Figs.1 and 2. Disconnected triangles (seven down and one up) in a) represent \bar{j} using non-integer values (seven rational and one irrational) of $1/F$, i.e. $F = 5/9, 2/(1 + \sqrt{5}), 5/8, 6/9, 6/8, 7/9, 7/8$ and $8/9$ at $\lambda = 0.1$. Different values of N_h , M and N_{phmax} were used to ensure that error bars, where not specified, are smaller than sizes of the symbols.

We summarize the overview of numerical results with a diagram describing different regimes, presented in Fig. 4(d), that are, in fact, all adiabatically connected. We distinguish four different regimes: i) the regime of damped free particle BO

(DBO) for small values of g , ii) critically damped (CD) regime where steady state current is reached in a time shorter than or of the order of t_B , oscillations in the current are still visible, however $j(t) > 0$ for any $t > 0$, iii) polaron BO regime (PBO) where system evolves nearly adiabatically, polaron Bloch oscillates within the polaron band and damping is exponentially small - numerically undetectable, and iv) damped polaron BO regime (DPBO) where remnants of PBO are seen in $j(t)$ while there exists a measurable average current $\bar{j} > 0$.

In summary we list our main results. Using a time dependent Lanczos method we have followed the time evolution of the polaron from its ground state towards the steady state after the electric field has been switched on. Different sizes of VHS have been used to ensure that presented results are valid in the thermodynamic limit. Steady state conditions have been reached at intermediate to high electric fields. Damped BO can be observed in the extremely weak EP coupling limit. In the former case, period of BO $t_B = 2\pi/F$ should be less than the relaxation time t_0/g^2 related with the emission of phonons. A large gap in the spectrum in the strong coupling regime is responsible for observation of nearly perfect BO arising from the polaron motion within the polaron band. Therefore, we expect that the breakdown of this quasiadiabatic regime resembles the Landau-Zener transition from the polaron band to higher excited states. Analytical estimate for the steady state current on the electric field and EP coupling constant at large fields is proposed and numerically tested.

We acknowledge stimulating discussions with C.D. Batista and financial support of the SRA under grant P1-0044. J.B. and L.V. acknowledge financial support of the REIMEI project, JAEA, Japan.

- [1] T. Oka, R. Arita, and H. Aoki, Phys. Rev. Lett. **91**, 066406 (2003).
- [2] H. Fehske, J. Schleede, G. Schubert, G. Wellein, V. S. Filinov, and A. R. Bishop, Phys. Lett. A **373**, 2182 (2007).
- [3] S. R. White and A. E. Feiguin, Phys. Rev. Lett. **93**, 076401 (2004).
- [4] J. K. Freericks, V. M. Turkowski, and V. Zlatic, Phys. Rev. Lett. **97**, 266408 (2006).
- [5] K. K. Thornber and R. P. Feynman, Phys. Rev. B **1**, 4099 (1970).
- [6] F. S. Khan, J. H. Davies, and J. W. Wilkins, Phys. Rev. B **36**, 2578 (1987).
- [7] D. Emin and C. F. Hart, Phys. Rev. B **36**, 2530 (1987).
- [8] S. Rott, N. Linder, and G. H. Döhler, Phys. Rev. B **65**, 195301 (2002).
- [9] J. Bonca and S. A. Trugman, Phys. Rev. Lett. **79**, 4874 (1997).
- [10] A. Johansson and S. Stafström, Phys. Rev. Lett. **86**, 3602 (2001).
- [11] D. M. Basko and E. M. Conwell, Phys. Rev. Lett. **88**, 056401 (2002).
- [12] A. A. Johansson and S. Stafström, Phys. Rev. B **69**, 235205 (2004).
- [13] J. Bonca, S. A. Trugman, and I. Batistic, Phys. Rev. B **60**, 1633 (1999).

- [14] J. Bonča, S. Maekawa, T. Tohyama, and P. Prelovšek, Phys. Rev. B **77**, 054519 (2008). (2010).
- [15] P. T. Jun and J. C. Light, J. Chem. Phys. **85**, 5870 (1986).
- [16] M. Mierzejewski and P. Prelovšek, Phys. Rev. Lett. **105**, 186405
- [17] O. S. Barišić, Phys. Rev. B **69**, 064302 (2004).